Micromachined Air-Lifted Pillar Arrays for Terahertz Devices

Cheolbok Kim, *Student Member, IEEE*, Daniel J. Arenas, David B. Tanner, and Yong-Kyu Yoon, *Member, IEEE*

***Abstract*— Micromachined air-lifted pillar arrays have been designed, fabricated, and characterized in the range of 1–3 THz. The pillar arrays consist of high-aspect-ratio epoxy structures defined by ultraviolet lithography followed by sputtered metallization. A Bruker 113v Fourier transform infrared spectrometer (FTIR) system has been used to characterize the fabricated air-lifted pillar arrays for both *p*- (*E*-field parallel to the plane of incidence) and *s*- (*E*-field perpendicular to the plane of incidence) polarized incident waves. Measurement results are verified using resonant frequency calculation and Floquet mode simulation. In the *p*-polarization measurement, the pillar arrays with a diameter of 5 μm, and heights of 28, 39, 54, and 60 μm show quarter wavelength resonant frequencies at 2.16, 1.81, 1.46, and 1.38 THz, respectively, as predicted. Since the air dielectric architecture has no dielectric loss, it would enable highly power efficient terahertz devices such as a monopole antenna, a frequency selective surface, and an electromagnetic absorber.**

***Index Terms*— Air-lifted pillar array, monopole antenna, frequency selective surface, absorber, terahertz, micromachining.**

I. Introduction

THE terahertz (THz) frequency gap (0.3 $\sim$ 3 THz) [1] lying between microwave and infrared frequencies has drawn much attention for the applications of biomedical imaging and security scanning with unique properties of deeper penetration than near-IR radiation, higher resolution than microwave/millimeter wave, low scattering, non-ionizing and non-invasiveness [2]. In the wireless communication fields, the THz spectrum offers advantages of device compactness and wide bandwidth, which would allow multi-gigabyte/sec indoor or inter-satellite communications [3].

Most THz devices [4], [5] by far, however, are patterned in a two dimensional (2-D) fashion on various dielectric substrates such as silicon, $YBa_2Cu_3O_{7-\delta}$, MgO and LT-GaAs and therefore suffer from dielectric loss and low radiation efficiency [6]. Often, low-loss dielectric materials such as alumina and zirconium-tin-titanate have been employed [7].

Recently, air-lifted, micromachined three dimensional (3-D) RF components have been reported for microwave and millimeter wave applications [8], [9]. The air dielectric 3-D architecture offers low dielectric loss, reduced substrate effects, and high radiation efficiency, which would greatly benefit THz devices since dielectric loss and low radiation efficiency are major drawbacks of current THz systems [1]. Meantime, the higher frequencies and the smaller characteristic dimensions lead to challenges in implementing 3-D architectures.

Manuscript received January 10, 2014; accepted January 23, 2014. Date of publication February 6, 2014; date of current version March 20, 2014. This work was supported in part by the NSF under Grant 1132413 and in part by the DoE under Grant DE-FG02-02ER45984. The review of this letter was arranged by Editor S. List.

C. Kim and Y.-K. Yoon are with the Department of Electrical and Computer Engineering, University of Florida, Gainesville, FL 32611 USA (e-mail: ykyoon@ece.ufl.edu).

D. J. Arenas is with the Department of Physics, University of North Florida, Jacksonville, FL 32224 USA.

D. B. Tanner is with the Department of Physics, University of Florida, Gainesville, FL 32611 USA.

Color versions of one or more of the figures in this letter are available online at http://ieeexplore.ieee.org.

Digital Object Identifier 10.1109/LED.2014.2303124

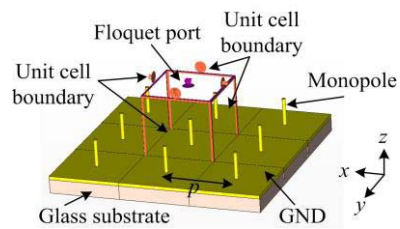

Fig. 1. Architecture of the air-lifted pillar array. For analysis, a unit cell with Floquet mode simulation is used.

In this letter, the polymer-core conductor process [9] is exploited to implement the THz high-aspect-ratio air-lifted pillar architecture using UV lithography and subsequent metallization. Since the vector network analyzer commonly used for microwave characterization is not readily available, in this study, an optical spectrometer approach using a Bruker 113v Fourier transform infrared spectrometer (FTIR) system is utilized for characterization. Measurement results are verified using analytical calculation and Floquet mode simulation with a commercial 3-D EM simulator (CST Microwave Studio, CST Inc.).

II. Design of Air-Lifted Pillar Array for THz

Fig. 1 shows the air-lifted pillar array architecture, where conductive pillars stick out of the ground plane. With the image theory, the incident EM wave maximally interacts with the pillars when the height of the pillar corresponds to the quarter wavelength of the EM waves. The quarter wavelength of 1–3 THz is in the range of 60 $\sim$ 20 μm. Here, the air-lifted pillars are defined by photolithography, where the thickness of the photoresist will be the ultimate height of the pillars. The photopatterning resolution is affected by the thickness of the photoresist and the wavelength of the UV source due to diffraction and proximity effects. The aperture size of the pillar mask should be greater than the minimum patternable size [10]:

$$d_{\min} = \frac{3}{2}\sqrt{\lambda_{UV}\left(s + \frac{1}{2}t\right)} \quad (1)$$

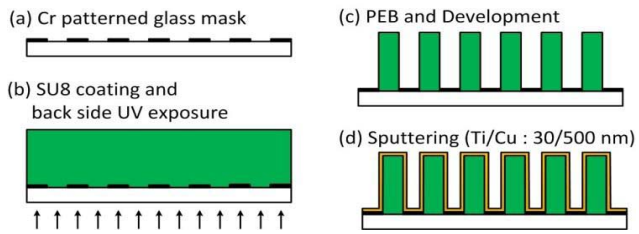

Fig. 2. Fabrication process of the pillar array.

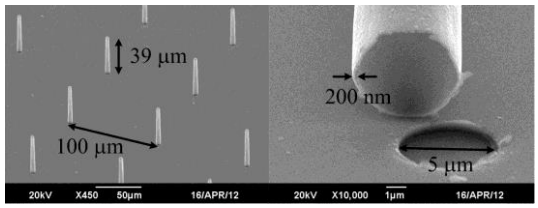

(a) (b)

Fig. 3. SEM pictures of (a) the pillar array and (b) the cross section view of a broken pillar showing 5 μm thick polymer-core enclosed by a 200 nm thick copper layer.

where $d_{\min}$ is the minimum diameter of the aperture, λ_{UV} is the wavelength of the UV lithography light source, s is the air gap between the mask and the photoresist, and t is the thickness of the photoresist. With contact-mode exposure, the air gap s can be zero, and $d_{\min}$ for i-line UV lithography ($\lambda_{\mathrm{UV}} = 365$ nm) will be 4.96–2.87 μm for 1-3 THz. So a photomask aperture size of 5 μm is selected for reliable pillar fabrication. Therefore, the aspect ratio of the air-lifted pillar is 1:12–4 for 1–3 THz.

III. Fabrication

The air-lifted pillar arrays are fabricated using the polymer-core conductor process (Fig. 2), which offers high-aspect-ratio conductor patterning capability, low cost, short fabrication time, and batch processibility [9]. A chromium (Cr) coated glass wafer is used both as a substrate and as a photomask. The Cr layer is patterned to define the pillar array using UV lithography and Cr etching (a). A negative tone photopatternable epoxy SU-8 (2025, Microchem, Inc.) is spincoated on top of the substrate, followed by softbake. The spin coating speed, baking time and temperature follow the standard recipe provided by the vendor (Microchem, Inc.). UV exposure is performed through the glass substrate, which justifies the zero gap contact-mode expose process (b). Post-exposure bake is performed, followed by development, after which the crosslinked pillar structures remain on the substrate (c). A thin film of titanium (Ti)/copper (Cu) (30 nm/500 nm) is deposited on the fabricated polymer structures using a sputtering system (Kurt J. Lesker CMS-18) (d).

Pillar arrays, with a pitch between pillars of 100 μm, a pillar diameter of 5 $\pm$ 0.5 μm and four heights of 28, 39, 54, and 60 μm, have been fabricated in 10 $\times$ 10 mm^2 area. The fabrication error in the pillar height for the pillars is maximum $\pm$6.0%. Fig. 3 shows scanning electron microscope (SEM) pictures of (a) a pillar array with a height of 39 μm and (b) the oblique view of a broken pillar. The breakage is made just for the thickness measurement purpose. The thickness of the coated copper on the SU-8 pillar is measured from the SEM image (Fig. 3(b)). The copper thickness on the substrate is approximately 500 nm while the thickness of 200 $\pm$ 30 nm is observed on the side wall of the pillar, which is attributed to the non-uniform conformal coating of the sputtering process. Note the side wall thickness of 200 nm of copper at 1.5 THz is more than three skin depths thick, and therefore the thickness is sufficient to serve as a good conductor as an equivalent solid counterpart.

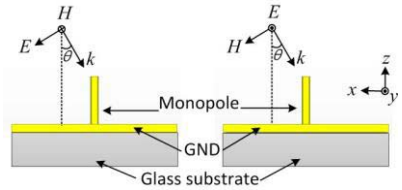

(a) (b)

Fig. 4. Incident waves for THz characterization: (a) p-polarization and (b) s-polarization.

IV. Characterization

The reflectance of the air-lifted pillar array is simulated in the range of 1–3 THz (wavenumbers of 30 $\sim$ 100 cm^{-1}) using a commercial EM 3-D simulator (CST Microwave studio, CST Inc.). The single unit cell used for simulation is shown in Fig. 1. The left/right (y-z plane) and front/back (x-z plane) faces are assigned as unit cell boundary conditions and a Floquet port is placed on the top face (x-y plane) of the boundary box. The simulation results represent ones from an infinite pillar array with a tilted incident wave. The side views of the tilted incident wave at the Floquet port with p- or s-polarization are shown in Fig. 4(a) and (b), respectively, with the tilting angle of the incident waves of θ.

The spectroscopy based reflectance of the air-lifted pillar arrays is measured using a Bruker 113v FTIR system with a resolution of 0.03 THz (1 cm^{-1}). A blackbody mercury-lamp, a 12 μm Mylar film, and a 4.2 K cooled silicon bolometer were used as the THz broadband source, beamsplitter, and detector, respectively. A wire-grid polarizer was used to differentiate the p- and s-polarization. The inset of Fig. 5(b) shows a diagram of the reflectance setup in the Bruker 113v. The THz incident beam is focused on the sample at an incident angle (θ) of 8°. From the focusing mirrors, the angular spread (δ) of the beam is also 8°. A copper film with the same quality and thickness of the film where the pillars are built is used as a reference surface. The error in the reflectance measurements was around +/−1% mainly due to the signal/noise issue in the THz region.

Fig. 5(a) and (b) show the simulated and measured reflectance for different pillar heights of 28, 39, 54 and 60 μm with (a) p-polarization and (b) s-polarization. Since the air-lifted pillar array can absorb only the E_z component, the p-polarized incident wave is mainly absorbed at the resonant frequencies of the pillar arrays, and therefore the measured (simulated) resonances occur at 2.16 (2.25), 1.81 (1.76), 1.46 (1.36) and 1.38 (1.24) THz for the heights of 28, 39, 54 and 60 μm, respectively, as shown in Fig. 5(a), while the entire s-polarized incident wave is reflected at all frequencies as shown in Fig. 5(b). The measured (simulated) 0.8-reflectance bandwidth are 0.06 (0.03), 0.07 (0.03), 0.09 (0.03) and 0.08 (0.03) THz for the heights of 28, 39, 54 and 60 μm, respectively. The discrepancies in the magnitude and bandwidth between the simulated and measured reflectance in

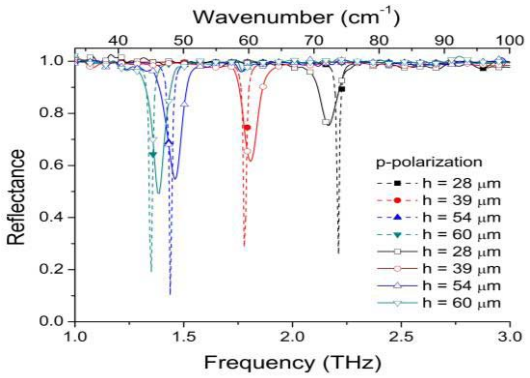

(a)

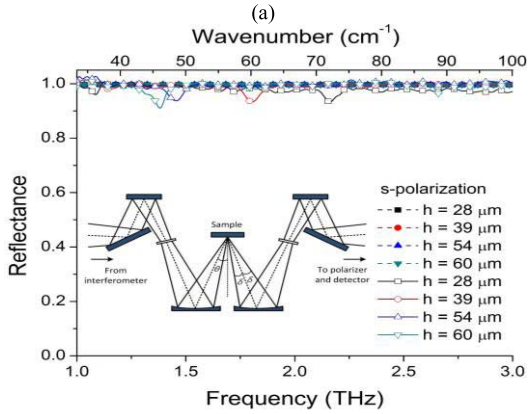

(b)

Fig. 5. The simulated and measured results with different heights of the pillar arrays for (a) p-polarized and (b) s-polarized incident wave. The dashed and solid lines are the simulated and measured results, respectively.

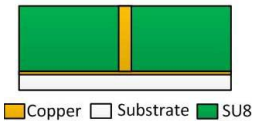

(a)

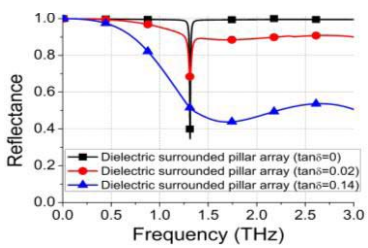

(b)

Fig. 6. (a) Geometry of the dielectric surrounded pillar and (b) its reflectance with different values of loss tangent.

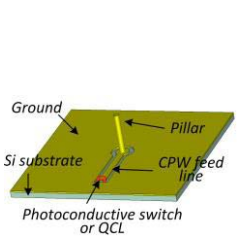

(a)

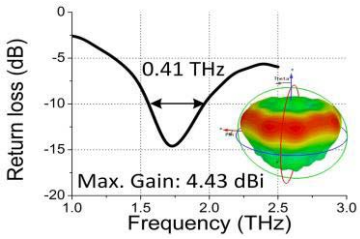

(b)

Fig. 7. Application of the air-lifted pillar: (a) a THz monopole antenna with a height of 40 μm and (b) its return loss and 3-D radiation pattern.

p-polarization are attributed to the fabrication tolerance and the conical shape of the THz beam. In the s-polarization measurement results, there are weak absorption peaks. Since the beam focused on the sample is pencil or cone shaped with a range of an angle deviation δ of $\pm$ 8°, there is always a small p-polarized component of the incident wave converging at the sample.

V. Conclusion

Micromachined air-lifted pillar arrays for terahertz applications have been demonstrated. They have been designed for 1-3 THz range and simulated by numerical means. The air-lifted pillar array is fabricated using the polymer-core conductor process, where UV lithography is used for patterning polymeric backbone and subsequent metallization is for electrical functionality. Uniform and high-aspect-ratio pillar arrays have been successfully fabricated. The fabricated air-lifted pillar arrays have been characterized using a Bruker 113v FTIR system in p- and s-polarization. The results of Floquet mode simulation show good agreement with the experimental data in the resonant frequencies of the pillar array and their response to p- and s-polarization. To estimate the effect of dielectric loss, a pillar array surrounded by a dielectric, SU8 ($\varepsilon_r = 3.2$, tan$\delta = 0.02/0.14$ @ 0.1/1 THz) [11] as shown in Fig. 6(a) has been simulated. The dielectric surrounded pillar array with zero loss tangent has the lowest reflectance at the resonant frequency of 1.3 THz and a complete reflection at the off-resonance frequencies while ones with a loss tangent of 0.02 and 0.14 have inferior reflectance performance at the resonance frequency and very high absorptions at the off-resonance frequencies due to dielectric loss as shown in Fig. 6(b). The demonstrated process can be applied for the air-lifted THz monopole antenna with the monopole separated from the ground plane as shown in Fig. 7(a), which would require an additional lithographical step. An omni-directional radiation pattern, a 10-dB bandwidth of 24 %, and a maximum gain of 4.43 dBi are simulated as shown in Fig. 7(b). This antenna will be especially useful for in-plane chip-to-chip communication applications.

References

[1] M. Tonouchi, "Cutting-edge terahertz technology," *Nature Photon.*, vol. 1, no. 2, pp. 97–105, 2007.

[2] A. Redo-Sanchez and X. -C. Zhang, "Terahertz science and technology trends," *IEEE J. Sel. Topics Quantum Electron.*, vol. 14, no. 2, pp. 260–269, Apr. 2008.

[3] C. Abou-Rjeily, "Pulse antenna permutation and pulse antenna modulation: Two novel diversity schemes for achieving very high data-rates with unipolar MIMO-UWB communications," *IEEE J. Sel. Area Commun.*, vol. 27, no. 8, pp. 1331–1340, Oct. 2009.

[4] J. V. Rudd, "Quadrupole radiation from terahertz dipole antennas," *Opt. Lett.*, vol. 25, no. 20, pp. 1556–1558, Oct. 2000.

[5] D.-T. Nguyen, F. Simoens, J.-L. Ouvrier-Buffet, *et al.*, "Broadband THz uncooled antenna coupled microbolometer array—Electromagnetic design, simulations and measurements," *IEEE Trans. Teraherts Sci. Technol.*, vol. 2, no. 3, pp. 299–305, May 2012.

[6] Y.-S. Jin, G.-J. Kim, and S.-G. Jeon, "Terahertz dielectric properties of polymers," *J. Korean Phy. Soc.*, vol. 49, no. 2, pp. 513–517, Aug. 2006.

[7] R. H. Bolivar, M. Brucherseifer, J. G. Rivas, *et al.*, "Measurement of the dielectric constant and loss tangent of high dielectric-constant materials at terahertz frequencies," *IEEE Trans. Microw. Theory Tech.*, vol. 51, no. 4, pp. 1062–1066, Apr. 2003.

[8] Y.-K. Yoon, B. Pan, J. Papapolymerou, *et al.*, "Surface-micromachined millimeter-wave antennas," in *Proc. 13th Int. Conf. Solid-State Sensors, Actuat. Microsyst.*, Jun. 2005, pp. 1986–1989.

[9] Y.-K. Yoon, J. W. Park, and M. G. Allen, "Polymer-core conductor approaches for RF MEMS," *J. Microelectromech. Syst.*, vol. 14, no. 5, pp. 886–894, Oct. 2005.

[10] W. Wang and S. A. Soper, *Bio-MEMS: Technologies and Applications*, 1st ed. Boca Raton, FL, USA: CRC Press, Dec. 2006.

[11] S. Lucyszyn, "Terahertz time-domain spectroscopy of film fabricated from SU-8," *Electron. Lett.*, vol. 37, no. 20, p. 1267, Sep. 2001.